Available online at www.sciencedirect.com

ScienceDirect

Procedia Structural Integrity 24 (2019) 658–666

Structural Integrity Procedia

www.elsevier.com/locate/procedia

AIAS 2019 International Conference on Stress Analysis

Thermographic applications for the rapid estimation of fatigue limit

Chiara Colombo[a]*, Laura Vergani[a]

[a] *Politecnico di Milano, Department of Mechanical Engineering, via La Masa 1, 20156 Milano, Italy*

Abstract

The AIAS group studying Energetic Methods for Experimental Analysis, MEAS, is performing round robin experimental tests for the rapid determination of fatigue limit on steels by different thermographic techniques. This work is part of the project and describes the experimental activity performed at Politecnico di Milano, based on stepwise cyclic tests. Thermograms are processed in terms of: 1) amplitude of the first order harmonic, in-phase with respect to the loading signal; 2) amplitude of the second harmonic, out-of-phase; 3) slope of the thermal signal with respect to the number of cycles. These values typically show bilinear trends, allowing to define a breakup point and a corresponding stress which is the thermographic estimation of the fatigue limit. The paper presents and discusses the results of tests with different stress ratios, i.e. fully reversed cycling with R=-1 and tensile-tensile cycling with R=0.1.

Keywords: Thermography; fatigue limit; experimental analysis.

1. Introduction

Several Italian groups have been working on the application of thermographic techniques to damage monitoring for several years, focusing their attention on the behavior of materials under fatigue loading.

The first researchers who faced this topic, La Rosa and Risitano (2000), proposed an innovative experimental technique to estimate the fatigue strength of homogenous steels by means of thermographic measurements. They, in particular, related the change in the thermal response of uniaxially loaded samples with the fatigue strength of

* Corresponding author. Tel.: +39-02-2399-8667; fax: +39-02-2399-8263.
E-mail address: chiara.colombo@polimi.it

10.1016/j.prostr.2020.02.058

homogeneous metals. Then, Curà et al. (2005) tested standard and notched samples and determined fatigue limit by a termographic method based on an iteration procedure. The fatigue limits obtained by thermographic methods were compared with the values obtained by means of staircase method following UNI Standards. Meneghetti (2007) proposed a parameter based on the energy dissipated in a unit volume of material and a theoretical model to derive the specific heat loss per cycle from temperature measurements.

More recently, different thermographic techniques were proposed and applied for the estimation of the fatigue limit of homogeneous materials. We can briefly cite some recent works, based on the analysis of:

- the mean temperature, in terms of thermal slope during the initial load application of cyclic tests, i.e. slope method, as in De Finis et al. (2015), or as the stabilized mean temperature, as in Risitano et al. (2015), and Corigliano et al. (2016);
- the thermoelastic sources, based on the first order harmonic, in-phase with respect to the forcing signal, Giancane et al. (2009) and Palumbo et al. (2017);
- dissipative thermal sources, based on the second order harmonic, out-of-phase with respect to the forcing signal, and on the heat energy dissipated in a unit volume of material per cycle, $\bar{Q}$, also in presence of propagating cracks, Meneghetti and Ricotta (2018).

The thermographic application of these techniques was extended from homogeneous to composite materials, such as to glass reinforced composites: Colombo et al (2012,a), Vergani et al (2014) and Colombo et al (2019); carbon reinforced composites: Pitarresi and Galietti (2010) and Pitarresi et al (2019); basalt reinforced composites: Colombo et al (2012,b). Thermographic techniques were applied also to hybrid steel-plastic panels, in Colombo et al (2015) and Colombo et al (2018), and to fiber metal laminates, in Montinaro et al (2017).

The present work is part of a project involving some Italian universities. We aim here to present the results from different thermographic techniques, applied to the monitoring of the steel specimens. Similar tests are being carried out on the same specimens in the labs of the different universities part of the project, with the aim of supporting the ability and robustness of any thermographic technique to identify rapidly and with precision the fatigue limit. All these estimations will be collected and discussed within the AIAS2019 conference, and validated by classical fatigue tests with the Staircase Method according with UNI 3964 standard. This project underlines the importance of thermography to accelerate the practical estimation of the fatigue limit, saving testing time, specimens and costs.

Nomenclature

E	elastic modulus
k	slope of the straight line in the Haigh diagram corresponding to a specific stress ratio
m	slope of the linear interpolations in the E-mode amplitude vs stress amplitude plot
n	total number of loading blocks, during stepwise tests
q	intercept of the linear interpolations in the E-mode amplitude vs stress amplitude plot
R	stress ratio, i.e. ratio between minimum and maximum stress applied during cycling
t	time
T	temperature
YS	yielding stress
UTS	ultimate tensile stress
ΔN	cycles performed for each loading block, during stepwise tests
$\Delta\sigma$	increase in maximum stress from two subsequent loading blocks, during stepwise tests
ε_F	strain at failure, from static tests
σ_a	stress amplitude
σ_{lim}	thermographic stress limit, estimated from the thermal trends during stepwise tests
σ_{max}	maximum stress
σ_0	stress of the first sinusoid loading block, during stepwise tests

2. Material and methods

Object of the work are the specimens given in Fig.1.a, nominally made of steel C45.

Two types of mechanical tests are performed:

1) Static tensile tests on 2 specimens, named MI-01 and MI-02. Static tests are carried out following ISO6892-1:2016 standard, with an extensometer having base of measure 25mm. The initial test speed is 1 mm/min up to ε=1%, then the secondary test speed is set to 2.5 mm/min after extensometer removal;
2) Stepwise tests, i.e. cyclic tests with variable stress amplitude. Stepwise tests consider blocks of 5000 cycles (ΔN) at 15Hz, and a maximum stress step between blocks of 15MPa (Δσ). Fig.2 shows a scheme of the loading blocks and Table 1 gives the details of each test. We investigated the effect of two stress ratios on the thermal response of this steel, by testing 2 specimens at R=-1 (named M1-03 and M1-04) and 2 specimens at R=0.1 (named M1-05 and M1-06). No extensometer is used during stepwise tests.

All the tests are performed with a servo-hydraulic testing machine (MTS Landmark) with 100kN load cell capacity, in a room with controlled temperature (T=25°C). The thermal camera is FLIR (Model: Titanium).

Fig.1.b shows the experimental setup adopted during both the static and the stepwise tests. The computer used to control the testing machine collects the load cell signal at the upper grip, and gives it to the lock-in port of the thermal camera. On the other hand, the thermal camera is connected with another laptop, acquiring both this lock-in signal and the thermograms with the software Altair. Sampling frequency during static tensile tests is 2 Hz, while for stepwise tests is 110Hz. The software used for the post-processing of stepwise data is AltairLI; both are commercial softwares by FLIR.

Thermograms collected during the stepwise tests are then processed considering:

- the mean temperature rise at the beginning of each block, i.e. slope method, processing the first 1000 cycles;
- the amplitude of the first order harmonic, in-phase with respect to the loading signal, i.e. the thermoelastic amplitude. This is commercially named E-mode in AltairLI;
- the amplitude of the second order harmonic, out-of-phase with respect to the loading signal, i.e. the thermoelastic amplitude. This is commercially named D-mode in AltairLI.

We processed the last 1000 cycles of each loading block for the analysis with the E- and D-mode.

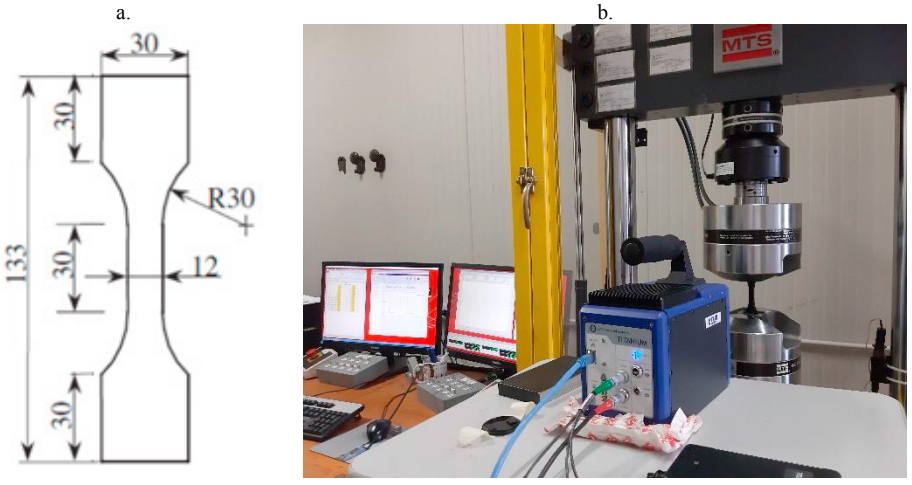

Fig. 1: a. Scheme of the specimens, with sizes in mm. Thickness is 6mm.
b. Setup of the static tensile and stepwise tests.

Table 1: Summary of the test parameters for the stepwise tests. $\sigma_{0,max}$ is the maximum stress of the first sinusoidal loading block; $\sigma_{0,a}$ is the amplitude of the first sinusoidal loading block.

	R	$\sigma_{0,max}$ (MPa)	$\sigma_{0,a}$ (MPa)	n, number of blocks
MI-03, MI-04	-1	200	200	15
MI-05, MI-06	0.1	305	137.3	26

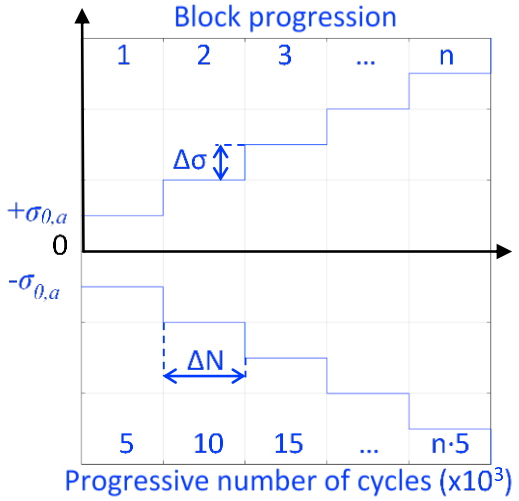

Fig. 2: Scheme of stepwise blocks for R-1.

3. Results of static tests

Fig.3 shows the results of the static tests from mechanical and thermal viewpoints. Fig.3.a shows the stress-strain curves of the two tested specimens. The two curves are overlapped and show a behavior characterized by an upper (initial peak) and lower yield stresses. Table 2 summarizes the mechanical outputs.

On the other hand, Fig.3.b shows the thermal trends, together with the stress ones, as a function of the test time. The temperature variation on the right axis is the average temperature over the whole area of the specimen (Fig.4.a) at the instant t, T(t), minus the initial average temperature on the same area at the beginning of the test, T(0). At the beginning of the test the temperature variation is decreasing, up to 22s which corresponds to the time to reach the yield stress: this is the well-known thermoelastic stage. Then, the temperature variation starts increasing, underlying yielding, necking and damage progression into the steel specimen. Both mechanical and thermal results are highly repeatable.

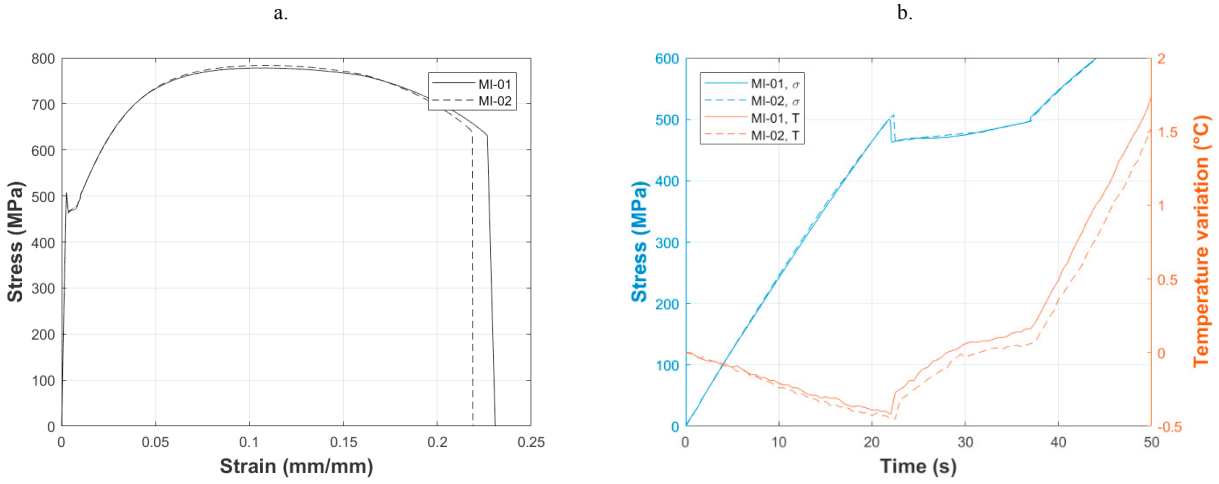

Fig.3: a. Stress-strain curves from static tensile tests;
b. Stress-time and Temperature-time curves at the beginning of static tensile tests.
The end of the decreasing thermal trend corresponds to the upper yield stress, at t=22s.

Table 2: Summary of mechanical results from static tensile tests.

	YS (MPa)	UTS (MPa)	E (GPa)	ε_F (mm/mm)
MI-01	463	778	209.8	0.227
MI-02	463	784	210.7	0.219

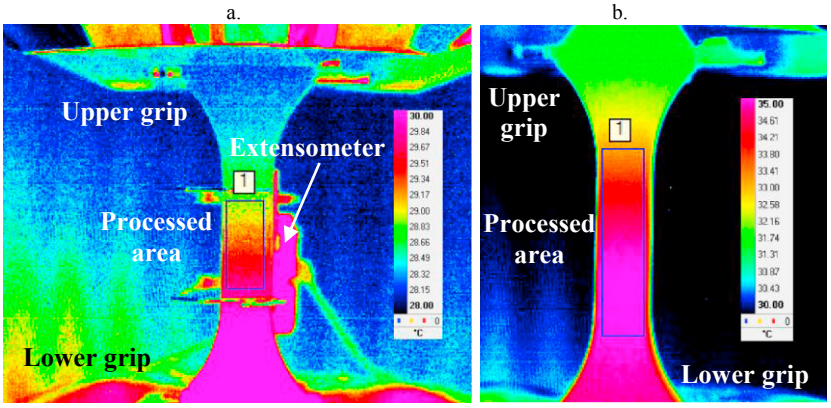

Fig.4: Thermograms of: a. specimen MI-01 under static load, at upper yield stress, testing time t=22s; b. specimen MI-04, tested at R=-1, in correspondence of $\sigma_{max}=\sigma_a$=320MPa. The central rectangle shows the processed area.

4. Results of stepwise tests

This section is dedicated to the post-processing of the thermal responses collected during stepwise tests. Two stress ratios are investigated: R=-1, i.e. fully reversed cycling, which is the classical stress ratio used for the definition of the fatigue limit with endurance tests, and R=0.1, i.e. tensile-tensile cycling. For all the specimens, the processed area corresponds to the central region, as shown in Fig.4.b.

4.1. Fully reversed cycling, R=-1

Figs.5.a-c show the results of the stepwise tests carried out at R=-1. The figures show the trends of E-mode module (Fig.5.a), D-mode module (Fig.5.b) and slope method (Fig.5.c) as a function of the maximum applied stress, which coincides in this case with the applied stress amplitude σ_a.

Table 3.a summarizes the regression coefficients of the bi-linear trends resulting from the interpolation of E-mode amplitude of Fig.5.a. The subscript 1 refers to the first interpolation lines of Figs.5.a-c, while the subscript 2 refers to the second interpolation lines (see Fig.5). Focusing on specimens MI-03 and MI-04, we can state that the points and the interpolating curves are really overlapped, i.e. m and q coefficients are very similar. Also, the determination coefficients of both the two interpolations are very near to the unit.

Table 3.a also shows the estimation of the fatigue limit by the three methods: 1) $\sigma_{lim,E}$ is the fatigue limit estimated by E-mode, as the intercept between the first and the second linear interpolation; 2) $\sigma_{lim,D}$ is the fatigue limit estimated by D-mode, as the last stress semi-amplitude having D-mode amplitude equal to 0; 3) $\sigma_{lim,slope}$ is the fatigue limit estimated by the slope method, as the last stress semi-amplitude before a net increase. All these values, for the two tested samples are very near. The average among these three estimations $\sigma_{lim,avg,R=-1}$ is similar for both samples, with an overlapped confidence interval between MI-03 and MI-04, based on the standard deviation. Despite the low number of tested samples, these results suggest that the test is repeatable and the methodology reliable.

4.2. Tensile-tensile cycling, R=0.1

Fig.5.d-f show the results of the stepwise tests carried out at R=0.1. The figures show the trends of E-mode module (Fig.5.d), D-mode module (Fig.5.e) and slope method (Fig.5.f) as a function of the applied amplitude σ_a.

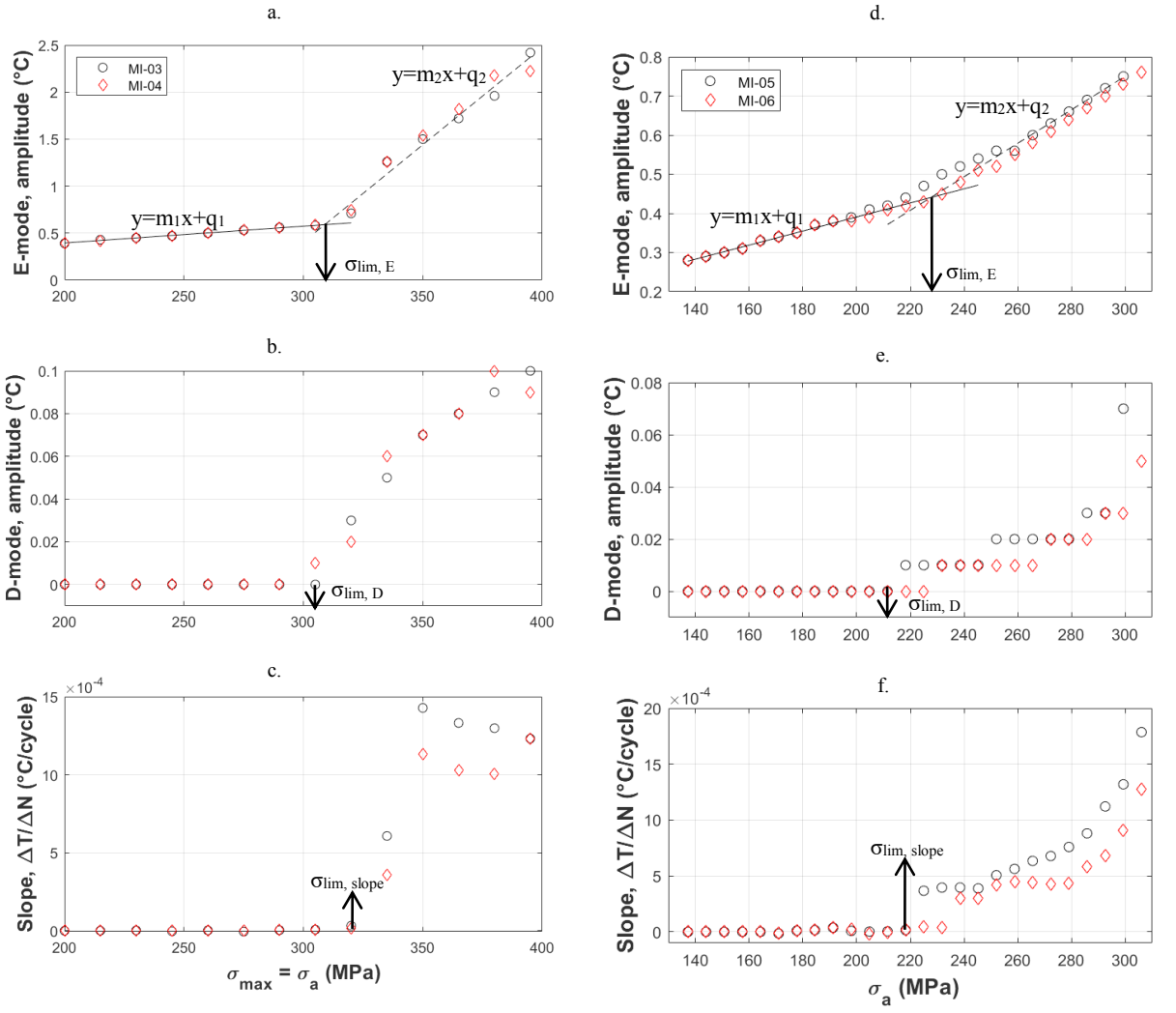

Fig.5: Plots of E-mode amplitude (a., d.), i.e. thermal amplitude of the in-phase harmonic, of D-mode amplitude (b., e.), i.e. thermal amplitude of the secondary harmonic, and of the slope ΔT/ΔN (c., f.), as a function of the applied semi-amplitude σ_a during each loading block.
a., b., c.: Results of MI-03 and MI-04 specimens, tested at R=-1.
d., e., f.: Results of MI-05 and MI-06 specimens, tested at R=0.1.

Table 3.b summarizes the regression coefficients from the interpolation of E-mode amplitude of Fig.5.f. As for the tested specimens at R=-1, also in this case the points and the related interpolating curves are overlapped, with determination coefficients near to the unit. The fatigue limit estimated by the three methods, given in Table 3.b, are quite similar, and $\sigma_{lim,avg,R=0.1}$ shows overlapped confidence interval between MI-05 and MI-06, meaning data repeatability.

Table 3: Summary of stepwise results for: a. R=-1; b. R=0.1.
m and *q* coefficients are the slope and intercept of the linear regression of the E-mode amplitude, as defined in Fig.5.a,d; R is the related coefficient of determination. $\sigma_{lim,E}$ is the fatigue limit estimated by E-mode; $\sigma_{lim,D}$ is the fatigue limit estimated by D-mode; $\sigma_{lim,slope}$ is the fatigue limit estimated by the slope method; $\sigma_{lim,avg}$ is the average of the fatigue limits estimated with the three methods.

a.

	MI-03	MI-04
m_1 (°C/MPa)	0.0018	0.0019
q_1 (°C)	0.0379	0.0138
R_1^2	0.9949	0.9984
m_2 (°C/MPa)	0.0207	0.0199
q_2 (°C)	-5.8070	-5.4825
R_2^2	0.9735	0.9589
$\sigma_{lim,E}$ (MPa)	309	305
$\sigma_{lim,D}$ (MPa)	305	290
$\sigma_{lim,slope}$ (MPa)	320	320
$\sigma_{lim,avg,R=-1}$(MPa)	311±8	305±15

b.

	MI-05	MI-06
m_1 (°C/MPa)	0.0018	0.0018
q_1 (°C)	0.0310	0.0340
R_1^2	0.9897	0.9877
m_2 (°C/MPa)	0.0043	0.0043
q_2 (°C)	-0.5350	-0.5535
R_2^2	0.9667	0.9294
$\sigma_{lim,E}$ (MPa)	228	235
$\sigma_{lim,D}$ (MPa)	212	225
$\sigma_{lim,slope}$ (MPa)	218	232
$\sigma_{lim,avg,R=0.1}$ (MPa)	219±8	231±5

4.3. Comparison and discussion

Based on the results of Par.4.1 and 4.2, it is evident that the two stress ratios have a deep effect not only on the fatigue life of the specimens, but also on their thermal response.

Comparing the E-mode trends of Fig.5.a,d. and Table 3, we can see that the initial slope (m_1 coefficient) is almost equal for all the tested samples, thus independent on the stress ratio R. This is correlated with the thermoelastic law and constant, i.e. the measured temperature is directly proportional to the applied stress. After the breakup points, the secondary slopes (m_2 coefficients) of the specimens tested at R=-1 are approximately 5 times higher than the ones of specimens tested at R=0.1. Also, the transition region at the breakup point between the two interpolation lines is quite different: R=-1 specimens have a net change of thermal behavior, and all the available points of Fig.5.a can be used for the regression of the first or the secondary lines. On the other hand, R=0.1 specimens show a smooth transition between the two lines, and some of the points of Fig.5.d in the range $220<\sigma_a<250$MPa have to be excluded from both the regressions. This smooth transition is typical of tests performed at R=0.1; indeed, in some works of our group performed in the past on composite materials, usually tested in tensile-tensile R=0.1 loading, we found very similar trends, Vergani et al. (2014).

Comparing the D-mode trend of Fig.5.b,e., we can identify clearly the initial region as fully flat, i.e. D-mode=0. Again, points corresponding to stresses beyond the fatigue limit have a different behavior. R=-1 specimens show a progressive increase of the D-mode, almost linear (Fig.5.b); R=0.1 specimens experience a much smoother increase, reaching only at the last block values of D-mode similar to R=-1 samples (Fig.5.e).

Finally, the comparison of the slope trends shows that the R=-1 specimens have a net gap before and after the fatigue limit, and the $\Delta T/\Delta N$ values remain quite constant beyond this applied stress (Fig.5.c). Also for R=0.1 samples of Fig.5.e there is a gap in the slope at the fatigue limit, but after this point the slope is constantly increasing.

Another interesting comment can be added to differentiate the thermal behavior of R=-1 and R=0.1 specimens. During the tests, R=-1 specimens warmed up to 230°C, while R=0.1 samples failed in correspondence of 65°C.

As a final comment, we can compare also the results of the fatigue limits estimated by the thermal analysis.

The fatigue limit of the specimens tested at R=-1, $\sigma_{lim,R=-1}$ =308MPa, averaged value between MI-03 and MI-04, can be analytically correlated to the average fatigue limit of the specimens tested at R=0.1, $\sigma_{lim,R=0.1}$, through Goodman's law and Haigh diagram (Fig.6):

$$\sigma_{\lim,\,R=0.1} = \frac{\left(\sigma_{\lim,\,R=-1}\right)\cdot UTS}{\left(k\cdot UTS\right)+\left(\sigma_{\lim,\,R=-1}\right)} \tag{1}$$

where *k* is the slope of the line corresponding to R=0.1 in Fig.6, defined as:

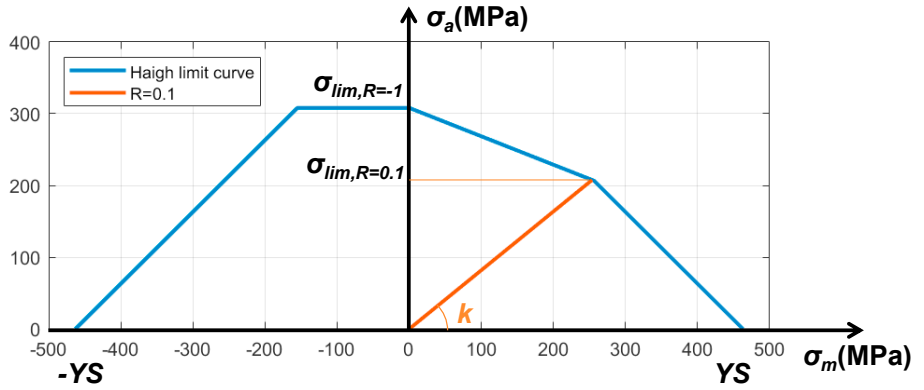

Fig.6: Simplified Haigh diagram.

$$k = \frac{(1-R)}{(1+R)} = \frac{0.9}{1.1} \tag{2}$$

The fatigue limit at R=0.1, according with Eq.1, is 208MPa. Fig.6 also shows the yielding limitation, which is near to Goodman's line for this mean stress value, but is not the limiting line for the estimation of the alternate fatigue limit. This value of $\sigma_{lim,R=0.1}$ is near to the thermographic value, averaged between MI-05 and MI-06, which is 225±9 MPa. Given these values, we can observe that the thermographic estimation of the fatigue limit with a stress ratio different from R=-1 is in line with the theoretical estimation from Haigh diagram. This could be a further proof of the validity of thermographic approach to estimate the fatigue limit.

5. Conclusions

The work presented the results of experimental tests carried out on steel specimens, thermographically monitored. The surface temperature field of the specimen was collected and analyzed during static and stepwise tests, i.e. cyclic tests with progressive increase in stress amplitude. The thermal trend during static tests simply identifies the yield stress. On the other hand, results from stepwise tests are more interesting:

- based on three thermographic techniques, we could identify a breakup stress amplitude, able to discern two different thermal behaviors. We propose, according with literature, that this is the fatigue limit of the material.
- tests carried out at R=-1 and at R=0.1 have a similar thermal behavior in the first part of the test, but quite a different one after that the damage occurs. However, the stress limits estimated by thermography for these stress ratios can be related by means of Haigh diagram.

Acknowledgements

The authors thank prof. Antonio Salerno from Politecnico di Milano for his support with the experimental testing and the Master student Mauro Sansone for processing part of the thermal data.

References

Colombo, C., Bhujangrao, T., Libonati, F., Vergani, L., 2019. Effect of delamination on the fatigue life of GFRP: A thermographic and numerical study. Composite Structures 218, 152-161.

Colombo, C., Carradó, A., Palkowski, H., Vergani, L., 2015. Impact behaviour of 3-layered metal-polymer-metal sandwich panels. Composite Structures 133, 140-147.

Colombo, C., Harhash, M., Palkowski, H., Vergani, L., 2018. Thermographic stepwise assessment of impact damage in sandwich panels. Composite Structures 184, pp. 279-287.

Colombo, C., Libonati, F., Vergani, L., 2012,a. Fatigue damage in GFRP. International Journal of Structural Integrity 3(4), 424-440.
Colombo, C., Vergani, L., Burman, M., 2012,b. Static and fatigue characterisation of new basalt fibre reinforced composites. Composite Structures 94(3), 1165-1174.
Corigliano, P., Crupi, V., Epasto, G., Guglielmino, E., Risitano G., 2016. Fatigue life prediction of high strength steel welded joints by Energy Approach. Procedia Structural Integrity 2, 2156–2163.
Curà, F., Curti, G., Sesana, R. 2005. A new iteration method for the thermographic determination of fatigue limit in steels. International Journal of Fatigue 27(4), 453-459.
De Finis, R., Palumbo, D., Ancona, F., Galietti, U., 2015. Fatigue limit evaluation of various martensitic stainless steels with new robust thermographic data analysis. International Journal of Fatigue 74, 88-96.
Giancane, S., Chrysochoos, A., Dattoma, V., Wattrisse, B., 2009. Deformation and dissipated energies for high cycle fatigue of 2024-T3 aluminium alloy. Theoretical and Applied Fracture Mechanics 52(2), 117-121.
La Rosa, G., Risitano, A., 2000. Thermographic methodology for rapid determination of the fatigue limit of materials and mechanical components. International Journal of Fatigue 22, 65-73.
Meneghetti, G., 2007. Analysis of the fatigue strength of a stainless steel based on the energy dissipation. International Journal of Fatigue 29, 81-94.
Meneghetti, G., Ricotta, M., 2018. The heat energy dissipated in the material structural volume to correlate the fatigue crack growth rate in stainless steel specimens. International Journal of Fatigue 115, 107-119.
Montinaro, N., Cerniglia, D., Pitarresi, G., 2017. Flying Laser Spot Thermography technique for the NDE of Fibre Metal Laminates disbonds. Composite Structures 171, 63–76.
Palumbo D., De Finis, R., Demelio, G.P., Galietti, U., 2017. Study of damage evolution in composite materials based on the Thermoelastic Phase Analysis (TPA) method. Composites Part B: Engineering 117(15), 49-60.
Pitarresi, G., Galietti, U., 2010. A Quantitative Analysis of the Thermoelastic Effect in CFRP Composite Materials. Strain 46, 446–459.
Pitarresi, G., Scalici, T., Catalanotti, G., 2019. Infrared Thermography assisted evaluation of static and fatigue Mode II fracture toughness in FRP composites. Composite Structures 226(15), 111220.
Risitano, A., La Rosa, G., Geraci, A., Guglielmino, E., 2015. The choice of thermal analysis to evaluate the monoaxial fatigue strength on materials and mechanical components. Proceedings of the Institution of Mechanical Engineers, Part C: Journal of Mechanical Engineering Science 229(7), 1315–1326.
Vergani, L., Colombo, C., Libonati, F., 2014. A review of thermographic techniques for damage investigation in composites. Frattura ed Integrità Strutturale 8(27), 1-12.